

PREPARED FOR SUBMISSION TO JCAP

Constraints on long-lived di-baryons and di-baryonic dark matter

Glennys R. Farrar and Zihui Wang

Center for Cosmology and Particle Physics, Department of Physics, New York University,
New York, NY 10003, USA

E-mail: gf25@nyu.edu, zihui.wang@nyu.edu

Abstract. A color-flavor-spin singlet state of six quarks $uuddss$ (S , or sexaquark) has been argued to be a potentially undiscovered deeply bound, long-lived hadron. Theoretical calculations of the S mass have been made in the literature, widely varying from deeply-bound ~ 1.2 GeV to weakly-bound ~ 2.2 GeV. Given the spread of the mass predictions, it is vital to derive observational constraints on the state as a function of the mass. The transition rates between S and two baryons are governed by \tilde{g} , the effective Yukawa coupling between S and two baryons with the same quantum numbers as S . In this paper, we place strong observational constraints on \tilde{g} , improving on various previous limits; additional limits assuming S is dark matter are also presented.

Contents

1	Introduction	2
2	Landscape of S phenomenology	3
2.1	Interactions of S	3
2.2	Mass and phenomenology	4
3	Stability of nuclei	7
3.1	Decay of deuterons	8
3.2	Experimental constraints from SNO	9
3.3	Other constraints	10
4	Stability of sexaquark dark matter	11
4.1	$S \rightarrow nn$	12
4.2	$S \rightarrow De\nu$	14
4.3	$S \rightarrow n\Lambda$	14
5	Laboratory limits on S production	14
5.1	Doubly-strange hypernuclei	15
5.2	Diffraction dissociation	16
5.3	Upsilon decay	16
5.4	Cooling of SN1987a	17
6	Isgur-Karl model of \tilde{g}	17
7	Critics review	18
7.1	Short-distance repulsion between baryons	19
7.2	S and oxygen stability	19
7.3	S and neutron stars	19
7.4	Relic abundance of S	20
7.5	Direct detection, CMB and S DM	20
8	Summary	20
A	Non-thermalization of S in the early Universe	21
B	Color-spin-flavor wavefunction projection	22
C	Cooling of SN1987a	22
D	$S \rightarrow \Lambda p \pi$	23

1 Introduction

The possibility that a deeply-bound *uuddss* sexaquark (S) with two units of baryon number may be an undiscovered stable hadron is advocated in [1, 2]. Unlike the case for bound states of two flavor octet baryons, Fermi statistics does not prevent all 6 quarks from being in a fully symmetric spatial configuration. Moreover, as a singlet simultaneously under color, spin and flavor, the color magnetic binding between quarks is maximal because the relevant quadratic Casimir operators vanish, as pointed out by Jaffe [3]. Using the MIT bag model, Jaffe calculated the mass of the lightest such state, the H-dibaryon, to be 2150 MeV; this mass is high enough to allow singly-weak decay, giving the H-dibaryon a lifetime estimated to be of order 10^{-10} s [3] but later calculated to be of order 10^{-8} s [4]. Subsequent mass predictions using a variety of models gave results spanning from 1.2 GeV to heavier than 2.2 GeV, thus leaving open the possibility of a deeply bound state with a cosmologically long lifetime in the event of a mass less than $m_\Lambda + m_n$ [5] or absolutely stable if it is lighter than two nucleons. The mass estimates are reviewed in greater detail in Sec. 2.

The deeply-bound S , if it exists, is distinct from and completely orthogonal to a weakly bound H-dibaryon composed of *uuddss*. Experiments creating doubly-strange hypernuclei and observing the decay products of Λ 's [6–9], showed that the formation time of an H is longer than the Λ lifetime. This would not be the case for a loosely bound, “molecular” H-dibaryon, unless its binding energy is less than the binding energy of two Λ 's in the hypernucleus, where $B_{\Lambda\Lambda} \approx 7$ MeV in ${}^6_{\Lambda\Lambda}\text{He}$ [8]). Thus these experiments exclude the existence of a weakly-bound *uuddss* state with mass between $m_n + m_\Lambda = 2054$ MeV and 2223.7 MeV [8]. The latest lattice QCD calculations [10, 11] show either a very weakly bound $\Lambda\Lambda$ molecule or above-threshold resonance, consistent with the hypernuclear experiments and an ALICE $\Lambda\Lambda$ phase-shift analysis [12]. In the following, we are not concerned with the H-dibaryon, but rather we constrain a possible compact, spatially symmetric, deeply bound state of the same quarks, designated S .

Ref. [13] studied the formation of S at the QCD phase transition in the early Universe using statistical mechanics and found that the abundance of S is comparable to that of ordinary baryons, and that with a sufficiently small breakup cross section the sexaquark component of the baryon asymmetry could survive the hot hadronic phase. Studies by [14, 15], assumed that S would thermalize with ordinary baryons in the hot hadronic phase of the early Universe and obtained the thermal evolution of S . Kolb and Turner [15], taking breakup reactions $XS \leftrightarrow BB'^1$ to have a typical hadronic cross section $\sim 1/m_\pi^2$, concluded that the density of S today is at most 10^{-10} that of ordinary baryons but if S exists it is an interesting relic. It is however worth noting that in Ref. [15] Kolb and Turner noted two scenarios in which S can have a significant dark matter (DM) relic density. In the first scenario, S must be lighter than 1.2 GeV, in accordance with [14]. However as we show in Sec. 2, this light mass scenario is not viable because it leads to the transition of two bound nucleons in a nucleus into S and a kaon with singly-weak lifetime, and is therefore ruled out by the stability of nuclei. In the second scenario, the one advanced in Ref. [13], the S breakup cross sections must be orders of magnitude smaller than $1/m_\pi^2$ to prevent S from coming into chemical equilibrium with baryons. Ref. [13] argued that such small breakup cross sections can arise naturally because the effective Yukawa coupling of S with two baryons that have identical quantum numbers as S (such as $\Lambda\Lambda$), denoted \tilde{g} may be very small. Details of that

¹Examples are $KS \leftrightarrow p\Lambda$, $\pi S \leftrightarrow \Sigma\Lambda$, $\gamma S \leftrightarrow \Lambda\Lambda$ and $\pi\pi S \leftrightarrow \Lambda\Lambda$. Note that $\pi S \leftrightarrow \Lambda\Lambda$ is forbidden by isospin conservation.

argument are given in appendix A. The generic Feynman diagram for $XS \rightarrow BB''$ including the Yukawa vertex is shown in figure 1.

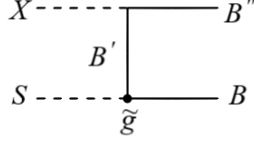


Figure 1: The effective Feynman diagram for $XS \rightarrow BB''$. The lower vertex, \tilde{g} , is an effective Yukawa vertex for S dissociating to two baryons that have the same quantum numbers as S (e.g. $\Lambda\Lambda$, $\Sigma^+\Sigma^-$ or ΞN).

Given the wide variance in m_S prediction using different theoretical calculation techniques (1.2 GeV - 2.23 GeV) and the possibility that S could be produced in the early Universe, we are motivated to derive observational constraints on \tilde{g} in the entire mass window 1.2 GeV - 2.23 GeV. The potential that a sufficiently small \tilde{g} may permit a relic abundance of S sufficient to compose up to 100% DM adds further motivation to study \tilde{g} . The Yukawa coupling \tilde{g} governs the transition between S and two baryons and produces a rich landscape of phenomenology. For instance, if m_S is lighter than two bound nucleons, a nucleus could decay to S and the rate is governed by \tilde{g} . We discuss under what circumstances the S is consistent with constraints on the stability of nuclei. If S is furthermore to be the DM, the possibility of its decay to baryons throughout cosmic history generates observable effects and we derive additional limits on \tilde{g} based on this consideration. It should be stressed that the scattering cross section between S and baryons is expected to be of order mb [1, 2] and is not related to \tilde{g} .

Our paper is organized as follows. In Sec. 2, we overview the phenomenology of S in different regimes of m_S and present the main result of the paper — the excluded region of \tilde{g} as a function of m_S . Section 3–5 are dedicated to deriving the various observational limits on \tilde{g} ; in Sec. 3 we constrain the decay of the deuteron to S and obtain strong limits from the Sudbury Neutrino Observatory (SNO) experiment; in Sec. 4, we analyze the signatures of S DM decaying to two baryons; in Sec. 5, we review the previous searches for the H-dibaryon and assess their sensitivity to \tilde{g} . In Sec. 6 we discuss a possible model that predicts a small \tilde{g} . Finally, we end with a review of existing literature on S in Sec. 7.

2 Landscape of S phenomenology

2.1 Interactions of S

Due to baryon number conservation, there are only two types of effective strong-interaction vertices of S on the hadron level. The first type is a Yukawa vertex that transfers baryon number between two baryons, B and B' , and S , where the two baryons have identical net quantum numbers as S . The other type is a vertex where S emits or absorbs a flavor singlet meson, predominately a vector meson V^μ .² Interactions of S can therefore be modeled by

²Since the S is a singlet in flavor, it cannot emit a flavor-octet meson without transitioning to a much more massive non-singlet di-baryon. The flavor-singlet combination of the ω and ϕ [13] vector mesons is the most important, because while the scalar meson $f_0(500)$ is lighter, it is a loosely-bound di-pion [16] or tetraquark, hence should have very small coupling to a deeply S which would be very compact, unlike a possible loosely bound di- Λ molecule resembling the deuteron and having mass $\approx 2m_\Lambda$.

the following hadron-level effective Lagrangian

$$\mathcal{L}_{\text{eff}} \supset \frac{\tilde{g}}{\sqrt{40}} \bar{\psi}_B \gamma^5 \psi_{B'}^c \phi_S + g_{SSV} \phi_S^\dagger \partial_\mu \phi_S V^\mu + \text{h.c.}, \quad (2.1)$$

where the superscript c denotes charge conjugation $\psi^c = -i\gamma^2\psi^*$. The first term is a Yukawa interaction with coupling constant $\tilde{g}/\sqrt{40}$. Here, \tilde{g} is the dynamical transition amplitude between six quarks in an S and in two baryons as introduced in Sec. 1. The Clebsch-Gordan factor $\sqrt{1/40}$ results from the color-spin-flavor wavefunction projection between S and individual color-singlet di-baryon states [17]; details are given in appendix B. An important fact is that in the fully-antisymmetrized S wavefunction, only $\sqrt{1/5}$ of the amplitude is contributed by a product of two color-singlet baryons; the other $\sqrt{4/5}$ is composed of products of color-octet states [17]. That $\sqrt{1/5}$, combined with the fact that there are 8 distinct flavor octet spin-1/2 baryons, accounts for the factor $1/\sqrt{40}$ appearing in eq. (2.1). The second term in eq. (2.1) accounts for the coupling of S to vector mesons. The phenomenology of the two types of interactions is distinctively different. The Yukawa interaction governs the transition between S and two baryons, and is relevant to processes such as the decay of S to two baryons and formation of S in exclusive scattering reactions. In contrast, the vector vertex gives rise to scattering of S with other hadrons through the exchange of vector mesons, which can be constrained by DM direct detection experiments and cosmology [18, 19]. For this paper, we concentrate on the phenomenology arising from Yukawa vertices proportional to \tilde{g} .

2.2 Mass and phenomenology

Theoretical and lattice computations done by different groups yield a wide spread of estimated S mass, ranging from deeply-bound, loosely-bound and unbound [3, 10, 20–29]. On the low end, the recent QCD sum rule calculation [30] obtained $m_S \approx 1200$ MeV. Values of 1200 and 2170 MeV were found in [14] using diquark models with different means of estimating parameters. A prediction of 1750 MeV is made by Ref. [31] in holographic QCD. Ref. [32] obtains a mass ≈ 1890 MeV by fitting the chromo-magnetic interactions between diquarks. For other earlier estimates see [2]. The NPLQCD lattice QCD mass calculation [28] had a very large pion mass (≈ 800 MeV) so is indicative at best, but found binding of about 80 MeV relative to two Λ 's, consistent with Jaffe's bag model prediction. The more recent Mainz group calculation [11] using the Luscher method reduced the pion mass to below 500 MeV and predicted a weak binding of ~ 5 MeV. The HALQCD group finds attraction, but insufficient to form a bound state [10]. The HALQCD method seeks to identify bound states by measuring the scattering amplitude of two hadrons and solving the Bethe-Salpeter equation to infer the potential. It is only applicable to weakly bound states due to their locality approximation [10], so would not be expected to detect an S . Moreover the $1/40$ probability of the S appearing in products of color-singlet baryons used – $|\Lambda\Lambda\rangle$, $|\Sigma\Sigma\rangle$ and $|\Xi N\rangle$ – discussed above, means that the scattering states explored in all existing lattice calculations have weak overlap with the S , making it even harder to see a signal.

The large variance in estimating m_S motivates us to consider the entire possible mass range below $2m_\Lambda$. From lower m_S to higher, the landscape of phenomenology is elaborated below and summarized schematically in figure 2.

1. For $m_S < 2m_N - m_K \approx 1382$ MeV, two nucleons in a nucleus could be converted to an S and a kaon via a singly-weak process, raising tension with the known stability of nuclei. Besides, stability of neutron stars excludes light baryonic states below 1.2

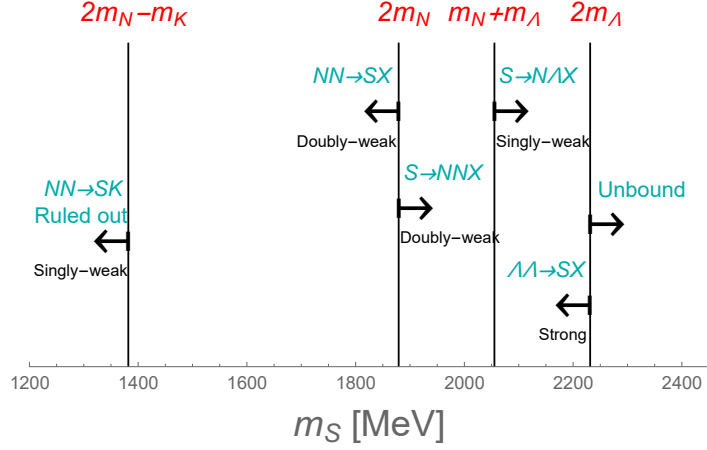


Figure 2: A schematic summary of the landscape of S phenomenology. Each vertical line indicates a critical mass scale where certain reactions are allowed. Note that the mass of a nucleon is coarsely denoted by $m_N \approx 938$ MeV here, with the mass splitting between the proton and neutron, the binding energy of nucleons inside a nucleus, and the mass of additional e^\pm neglected in this figure. From left to right: singly-weak transitions $NN \rightarrow SK$, doubly-weak transitions $NN \rightarrow SX$; doubly-weak decays $S \rightarrow NNX$; singly-weak decays $S \rightarrow N\Lambda X$; strong-interaction transitions $\Lambda\Lambda \rightarrow SX$; unbound (a broad resonance).

GeV [33, 34], and a light scalar S would worsen the instability because it does not have Fermi pressure.³ Therefore, we consider $m_S \lesssim 1382$ MeV as observationally ruled out.

2. If $1382 \text{ MeV} < m_S < 2m_N - B_{NN}$, where B_{NN} is the 2-nucleon binding energy, the doubly-weak decay of a nucleus to an S can give observable signatures. We will use the e^\pm searches at the SNO experiment to constrain deuteron decaying to S and thereby place the strongest limits on this mass range. This updates the analysis of [5] based on estimation of the sensitivity of SuperK to ^{16}O decay.
3. The narrow mass range in which an S is too light to decay to a deuteron or free nucleons, while at the same time is heavy enough that nuclear stability is ensured, $m_D - m_e \leq m_S \leq m_D + m_e$ (or 1875.1 - 1876.1 MeV), is much less constrained. In practice, due to the narrow phase space and detection thresholds of low energy e^\pm , the mass window 1870 - 1880 MeV is hard to constrain by decay of nuclei or decay of S . The cooling of SN1987a and observations of hypernuclei provide the best bounds here.
4. If $m_S \gtrsim 2m_N$ but $m_S \lesssim m_n + m_\Lambda$, the S can decay to two-nucleon final states via a

³Ref. [35] showed that the observed neutron star mass-radius relationship, and neutron star masses above $2 M_\odot$, are compatible with the existence of a sexaquark with mass above $2m_N$ when quark deconfinement at high pressure is taken into account, as indeed is necessary with or without an S .

doubly-weak interaction. There are four principal channels:

$$S \rightarrow \begin{cases} De^- \bar{\nu}_e, & m_S \geq 1876.1 \text{ MeV}, \\ ppe^- e^- \bar{\nu}_e \bar{\nu}_e, & m_S \geq 1877.6 \text{ MeV}, \\ npe^- \bar{\nu}_e, & m_S \geq 1878.3 \text{ MeV}, \\ nn, & m_S \geq 1879.1 \text{ MeV}. \end{cases} \quad (2.2)$$

To be a DM candidate, the S lifetime must be at least longer than the age of Universe $t_{\text{univ}} = 1.37 \times 10^{10}$ yr [36]. Additionally, charged leptons in the decay final states may be observed in astrophysical or laboratory measurements, which we use here to set much stronger limits on \tilde{g} if S is a significant component of dark matter. If $m_S \gtrsim m_N + m_\Lambda \approx 2055$ MeV, singly-weak decays of S result in a much shorter lifetime.

5. As long as $m_S < 2m_\Lambda = 2231.4$ MeV, strong-interaction transitions $\Lambda\Lambda \rightarrow SX$ are allowed. These transitions can be constrained by observations of double- Λ hypernuclei [5–9] and by their impact on the cooling of supernovae [37].

Generically, the rate of all of the processes above are proportional to \tilde{g}^2 , since they either require the S to disintegrate to or be produced from two baryons.

Observational constraints on \tilde{g} , which are the main results of our paper, are summarized in figure 3. Here we briefly describe the figure, postponing the in-depth derivations to sections 3–6. The cyan line in figure 3 follows from our analysis of the deuteron decay $D \rightarrow Se\nu$, using data from the SNO experiment (Sec. 3). This improves significantly on the estimated upper limit based on SuperK sensitivity to oxygen decay [5], shown by the orange line. The green region is excluded by the observation of hyperon decay products from doubly-strange hypernuclei, thus placing a limit (reviewed in Sec. 5.1) on the formation time of S [5]. The red line is adapted from [37] and is the upper limit on \tilde{g} required for the observed cooling of SN1987a as discussed in Appendix C. Additionally, in Sec. 5 we recast the H-dibaryon searches from two accelerator experiments, BNL E888 and Belle; the resulting upper limits on \tilde{g} are respectively given by the dark red and dark blue lines. As noted in the detailed discussions which follow, e.g., Sec. 3.1, some of the bounds depend quite sensitively on the typical momenta of the virtual quarks involved in the process, p_q ; in figure 3 p_q is fixed to 100 MeV. The gray band is a representative theoretical prediction for \tilde{g} based on the Isgur-Karl model of spatial wavefunctions following [5], reviewed in Sec. 6.

The bounds on \tilde{g} discussed above apply whether or not S is the DM particle. If S constitutes part or all of the DM, four additional DM-based constraints can be obtained; these are shown by dashed lines in figure 3, taking DM to be entirely composed of S . The black line is the maximum value of \tilde{g} such that S does not come into chemical equilibrium with baryons in the early Universe, so that its relic abundance can be preserved to low redshift [13] (see also appendix A). The blue line indicates the value of \tilde{g} for which the lifetime of S is equal to the Hubble time. The brown line follows from requiring that the accumulation of deuterium since BBN, due to $S \rightarrow De\nu$, be consistent with the measured deuterium abundance in damped Lyman- α systems given the primordial D abundance predicted by Λ CDM with parameters from the CMB. The magenta region is ruled out by a new limit derived here based on the energy injection of S decay products to astrophysical systems including CMB [38], Lyman- α forests [39], and gas-rich dwarf galaxies [40]. If S is a fractional component of the DM, the dashed brown and magenta exclusions are weakened by a factor of $\sqrt{f_S}$ where f_S is the fraction of DM composed of S ; how the dashed black constraint depends on f_S requires a complete study of solving Boltzmann equations and is beyond the scope of this paper.

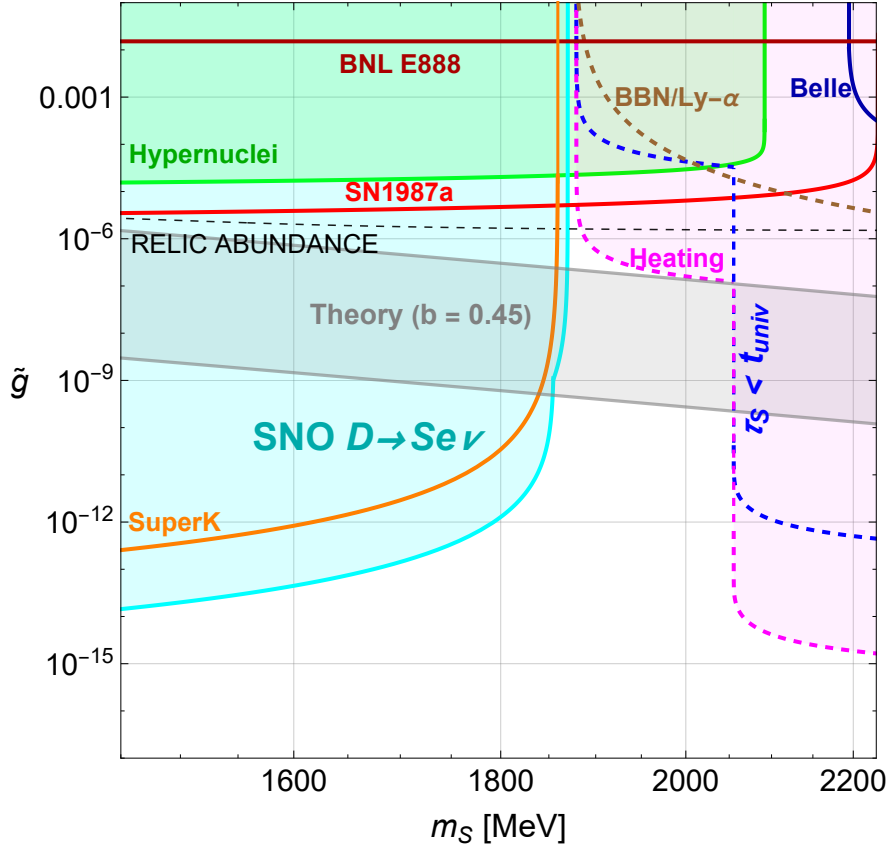


Figure 3: Excluded and predicted regions of \tilde{g} . The gray band is the theoretical best-estimate for \tilde{g} . The solid lines/regions are observational limits on \tilde{g} which do not require S to be DM. The dashed lines show DM-based constraints if DM is entirely made of S . See main text for detailed description and derivation for each limit. As discussed in the text, the exclusion regions are sensitive to the typical quark momenta in the process, taken to be 100 MeV here.

3 Stability of nuclei

The transition between a two-nucleon state and S (and additional leptons if necessary) must be doubly-weak to convert two units of strangeness. This motivates us to evaluate the matrix elements $\langle S|H_W|NN'\rangle$, where H_W is the effective Hamiltonian that characterizes the doubly-weak interaction. To proceed, we can insert a complete di-baryon state

$$\langle S|H_W|NN'\rangle = \sum_{BB'} \langle S|BB'\rangle \langle BB'|H_W|NN'\rangle. \quad (3.1)$$

Because $\langle S|BB'\rangle$ is only non-zero for eight particular color-singlet di-baryon states, in the exact flavor SU(3) limit where all octet baryons have an equal mass the matrix element sums to zero (see eq. (B.3) in appendix). In the presence of flavor breaking, the matrix element is dominated by the lightest di-baryon transition, i.e.,

$$\langle S|H_W|NN'\rangle \approx \frac{\tilde{g}}{\sqrt{40}} \langle \Lambda\Lambda|H_W|NN'\rangle. \quad (3.2)$$

The non-vanishing matrix elements $\langle S|H_W|NN'\rangle$ enable a number of reactions involving S and two nucleons. Notably, if S is light enough, two nucleons in a nucleus could be converted

to an S causing nuclei to be unstable. On the other hand, if S is heavy enough, it can decay to two nucleons.

3.1 Decay of deuterons

The three leading channels of nuclei decaying to S are

$$\begin{cases} pp \rightarrow Se\nu\nu & \Longleftrightarrow & (A, Z) \rightarrow (A-2, Z-2) + Se\nu\nu, \\ np \rightarrow Se\nu & \Longleftrightarrow & (A, Z) \rightarrow (A-2, Z-1) + Se\nu, \\ nn \rightarrow S & \Longleftrightarrow & (A, Z) \rightarrow (A-2, Z) + S. \end{cases} \quad (3.3)$$

The lightest nucleus that could decay to S is the deuteron D , via the reaction $D \rightarrow Se\nu$. The ground state of deuterons is dominated by $J = 1$ and $L = 0$, with a subdominant ($\sim 4\%$) component having $J = 1$ and $L = 2$ [41]. For our purposes we will neglect this admixture and restrict the discussion to $L = 0$.

Since an accurate modeling of $D \rightarrow Se\nu$ at the level of individual nucleons is difficult, we treat the deuteron as an effective vector field D^μ . The decay must be transmitted by two virtual W bosons, with one absorbed internally and one decaying to leptons. Thus, the coupling of D to the W boson and S can be modeled by

$$\mathcal{L} \supset \frac{\tilde{g}}{\sqrt{40}} g_{DSW} \phi_S^\dagger W_\mu D^\mu + \frac{ig_W}{2\sqrt{2}} W_\mu \bar{\psi} \gamma^\mu (1 - \gamma^5) \psi, \quad (3.4)$$

where g_W is the weak coupling constant defined by $G_F = \sqrt{2}g_W^2/(8m_W^2)$. The effective Feynman diagram for this decay at the hadron level is shown in the left panel of figure 4. We also show one example of quark-level diagrams in the right panel of figure 4. The coupling

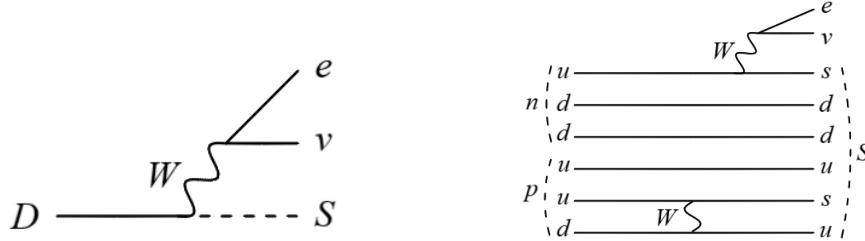


Figure 4: Feynman diagrams for $D \rightarrow Se^+\nu$ at the hadron level (left) and the quark level (right).

constant g_{DSW} encodes the exchange of an internal W boson and emission of the W ; it has dimension of mass. We can estimate it by

$$g_{DSW} \simeq g_W G_F p_q^3 \sin^2 \theta_C \cos \theta_C, \quad (3.5)$$

which follows from the bound state Bethe-Salpeter amplitude. Here θ_C is the Cabbibo mixing angle with $\sin \theta_C = 0.22$, and p_q is the characteristic momenta of quarks. The power of p_q follows from the construction and can be deduced on dimensional grounds based on the mass dimension of g_{DSW} being one, from the effective Lagrangian eq. (3.4). We note that the decay rate $\Gamma \propto g_{DSW}^2$ is highly sensitive to the numerical value of p_q . Throughout the paper, we will proceed with $p_q = \Lambda_{\text{QCD}} \simeq 100$ MeV. We note that p_q can take values up to the constituent

masses (for light and strange quarks, the constituent mass is roughly 340 MeV and 480 MeV respectively) and thus, the decay rate could be enlarged by a factor of $3.4^6 \simeq 1544$. Or conversely, if the mass difference between D and S is small, the effective momenta in the integrals might be smaller than 100 MeV. Therefore, the appearance of p_q^6 in the rate raises the major uncertainty in our modeling of D decay, and subsumes other subleading sources of uncertainties, such as the summation of different quark level diagrams.

We directly compute the decay amplitude from the effective Lagrangian eq. (3.4)

$$\langle |\mathcal{A}|^2 \rangle = \frac{g_{DSW}^2 g_W^2}{3m_W^4} (3E_e E_\nu - \vec{p}_e \cdot \vec{p}_\nu), \quad (3.6)$$

and the differential decay rate can be found by

$$\frac{d\Gamma}{dE_e d\Omega_e d\Omega_\nu} = \frac{1}{(4\pi)^5 m_D} \int dE_\nu \langle |\mathcal{A}|^2 \rangle. \quad (3.7)$$

This leads to

$$\frac{d\Gamma}{dE_e} = \frac{\tilde{g}^2 G_F^4 p_q^6 \sin^4 \theta_c \cos^2 \theta_c}{120\pi^3 m_D m_S} \sqrt{E_e^2 - m_e^2} E_e (m_D - m_S - E_e)^2. \quad (3.8)$$

Integrating over all possible positron energies $m_e \leq E_e \leq m_D - m_S$ yields the decay rate

$$\Gamma = \int_{m_e}^{m_D - m_S} dE_e \frac{d\Gamma}{dE_e}. \quad (3.9)$$

3.2 Experimental constraints from SNO

A stringent laboratory constraint on deuteron instability can be deduced from the SNO experiment. The SNO detector [42] contains 10^6 kg of heavy water, and the positrons produced in $D \rightarrow Se\nu$ would create Cherenkov radiation which can be detected by photomultipliers (PMTs) installed in the detector⁴. Figure 5 shows the expected energy spectrum of positrons from $D \rightarrow Se^+\nu$, for various values of m_S . The vertical black line at $E_e = 5.5$ MeV indicates the detection threshold. We also define the function $f(x)$ to be the fraction of positrons that have energy above $E_e = x$,

$$f(x) = \frac{\int_x^{m_D - m_S} dE_e d\Gamma/dE_e}{\int_{m_e}^{m_D - m_S} dE_e d\Gamma/dE_e}. \quad (3.10)$$

Two important values of x are, *i*) $x = 5.5$ MeV is the detection threshold, and *ii*) $x = 20$ MeV is the highest energy of e^\pm detected by SNO.

We require the positrons within 5.5–20 MeV produced by deuteron decay be less than the recorded e^\pm counts at SNO, and in addition, positrons higher than 20 MeV should be statistically consistent with the null result. We also make the conservative assumption that all the observed e^\pm events at SNO are due to deuteron decay. Therefore, we can set limits on the decay rate Γ by

$$\begin{cases} (f(5.5) - f(20)) \times N_0(1 - e^{-\Gamma t}) < N_{\text{obs}}, \\ f(20) \times N_0(1 - e^{-\Gamma t}) < 2.44, \end{cases} \quad (3.11)$$

⁴Although the PMTs are designed to detect electrons produced by solar neutrinos in the reaction $\nu_e + D \rightarrow 2p + e^-$, positrons would give the same signal because the spectrum of Cherenkov radiation is only sensitive to charge-squared.

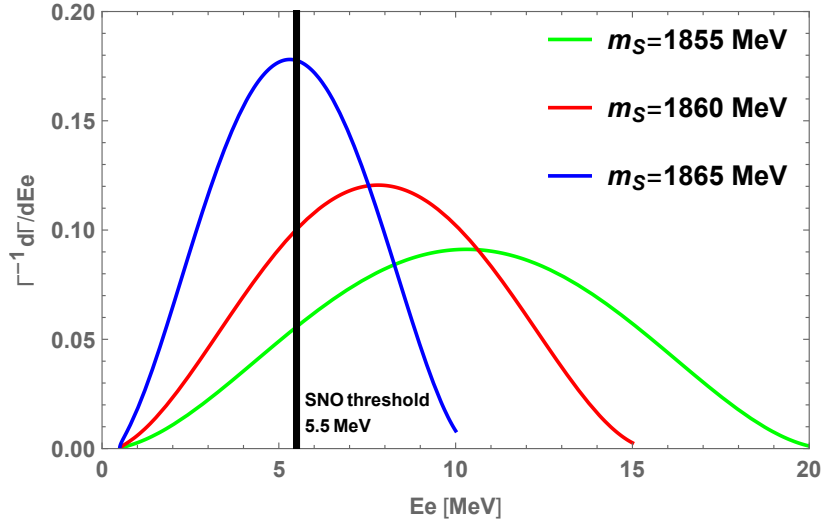


Figure 5: The expected energy spectrum of positrons, $\Gamma^{-1}d\Gamma/dE_e$ in unit of GeV^{-1} , produced in the deuteron decay $D \rightarrow Se^+\nu$ for $m_S = 1855, 1860$ and 1865 MeV. The solid black cutoff at $E_e = 5.5$ MeV is the threshold of e^\pm detection at SNO.

whichever is stronger. Here, $N_0 = 6.0138 \times 10^{31}$ is the number of deuterons in the SNO tank, $N_{\text{obs}} \approx 2465$ is the observed number of e^\pm events recorded during $t = 391.432$ days, and 2.44 in the second equation is the 90% confidence level upper limit consistent with null observation. With the expressions for Γ and $f(x)$ in eqs. (3.9, 3.11), this implies lower limits on \tilde{g} as a function of m_S . The resulting excluded region taking $p_q = 100$ MeV is plotted as the cyan area in figure 3. We also note that when $m_S \lesssim 1750$ MeV, new decay channels that include pions in the final state open up, so these limits on \tilde{g} could be strengthened for $m_S \lesssim 1750$ MeV. This is not highly motivated because the current limit is so strong relative to theoretical estimates, discussed below, that $m_S \lesssim 1750$ MeV already is strongly disfavored.

3.3 Other constraints

Deuteron decay can have other observational consequences in astrophysics. We give two examples below.

- The primordial abundance of deuterium, D/H , would be depleted at low-redshift relative to the BBN predicted value. Ref. [13] reports that the comparison of predicted and measured values of D/H indicates $\tau_D \gtrsim 5 \times 10^{14}$ yr. This is however much less stringent than our SNO analysis which indicates $\tau_D \gtrsim 10^{32}$ yr.
- Deuterium in the interstellar medium can decay to $Se^+\nu$ and produce positrons with $\mathcal{O}(\text{MeV})$ energies. This provides a potential solution to explain the Galactic 511 keV line observed by the INTEGRAL satellite [43]. Using the INTEGRAL implied upper limit on the positron injection rate $4 \times 10^{43}/\text{s}$ [44], we find $\tilde{g} \lesssim 3 \times 10^{-2}$. At present, this is a very weak limit on \tilde{g} .

Both of these limits are much weaker than the SNO limit and therefore, we refrain from showing them in figure 3.

Heavier nuclei with larger binding energies could also decay in similar ways. For example, Oxygen-16 could decay to Nitrogen-14 by $^{16}\text{O} \rightarrow ^{14}\text{N} + S + X$ if $m_S \lesssim 1862$ MeV. The

water tank at SuperK can in principle provide data to constrain the decay. However the existing analyses at SuperK focus on exclusive searches for e^\pm or pions with energy more than $\mathcal{O}(100 \text{ MeV})$ (see e.g. [45, 46]), and therefore these analyses are not relevant to S for which the positron energy of interest is $\mathcal{O}(\text{MeV})$. Ref. [5] estimated based on the SuperK noise level that an ^{16}O lifetime less than $\sim 10^{26} \text{ yr}$ would trigger the SuperK detector. It translates to the orange line in figure 3 and is superseded by our SNO limits. Future dedicated inclusive searches for di-nucleon decay events could be useful to place improved limits on S , and other baryon number violating processes [46] in broader contexts.

4 Stability of sexaquark dark matter

Evidence of DM has been observed from both early and late Universe phenomena and therefore, DM is believed to be stable on the cosmological timescale. For this reason, many models of DM make use of symmetries to stabilize DM particles so that they are perfectly stable. On the other hand, some popular DM candidate particles can decay and have a finite lifetime, such as axions [47] and sterile neutrinos [48], as long as the lifetime is consistent with observational constraints. Recently, decaying DM has also been motivated by various tensions in cosmology, including Hubble tension [49] and S_8 tension [50, 51].

In this section, we constrain \tilde{g} by studying the decay of SDM to two baryons. In particular, we will calculate the lifetime of doubly-weak decays $S \rightarrow D\bar{\nu}$ and $S \rightarrow nn$, and the singly-weak decay $S \rightarrow n\Lambda$. The effective diagram for $S \rightarrow D\bar{\nu}$ is similar to figure 4, with the position of D and S swapped. Figure 6 shows illustrative Feynman diagrams for $S \rightarrow nn$ and $S \rightarrow n\Lambda$ at the quark level.

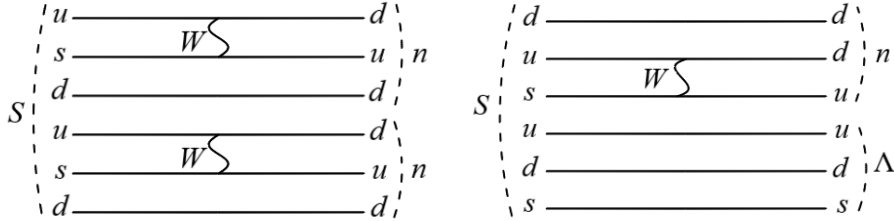


Figure 6: Left: An example of a quark diagram for the doubly-weak decay $S \rightarrow nn$. Right: An exemplary quark diagram of the singly-weak decay $S \rightarrow n\Lambda$.

For simplicity, we assume that DM comprises S solely. If S is a fraction f_S of the total DM density, the limits on \tilde{g} derived in this section are weakened by a factor of $\sqrt{f_S}$.

4.1 $S \rightarrow nn$

The effective Lagrangian for two-neutron decay of the S is a Yukawa interaction

$$\mathcal{L} \supset \frac{\tilde{g}}{\sqrt{40}} \bar{\psi}_n (g + ig_5 \gamma^5) \psi_n^c \phi_S, \quad (4.1)$$

with the decay rate

$$\Gamma = \frac{\tilde{g}^2 m_S}{640\pi} \left[g^2 \left(1 - \frac{4m_n^2}{m_S^2} \right)^{3/2} + g_5^2 \left(1 - \frac{4m_n^2}{m_S^2} \right)^{1/2} \right]. \quad (4.2)$$

Since this is a weak decay, one should expect both g and g_5 are non-zero. For our purpose here, however, we will take $g_5 = 0$ which yields the minimal decay rate and therefore the most conservative constraint. We estimate g by the Feynman diagram shown in the left panel of figure 6

$$g^2 \simeq G_F^4 p_q^8 \sin^4 \theta_c \cos^4 \theta_c, \quad (4.3)$$

leading to

$$\Gamma = \frac{\tilde{g}^2 G_F^4 p_q^8 \sin^4 \theta_c \cos^4 \theta_c m_S}{640\pi} \left(1 - \frac{4m_n^2}{m_S^2} \right)^{3/2}. \quad (4.4)$$

As before, we take p_q to be the QCD scale 100 MeV, and therefore $\Gamma \propto p_q^8$ dominates the uncertainty in our modeling of the decay rate.⁵

There are various astrophysical and cosmological constraints on decaying DM.

- Assuming that the lifetime of decaying DM should exceed the age of Universe, $\tau_{\text{DM}} > t_{\text{univ}} = 1.37 \times 10^{10}$ yr [36], from eq. (4.4) we find the blue region in figure 3 is excluded. However, if $\tau_{\text{DM}} = t_{\text{univ}}$, about 1/3 DM would have already decayed and the decay products would disturb low redshift astrophysical and cosmological observables. Thus, we can anticipate potentially much stronger limits on the lifetime, as discussed below.
- Neutrons from $S \rightarrow nn$ will undergo β -decay and produce electrons. The energy of these electrons is peaked around 1 MeV; it is only very weakly sensitive to the value of m_S . Constraints on DM decaying to e^\pm pairs have been extensively studied in literature [38–40, 52] based on energy injection from e^\pm to astrophysical systems. Among them, the strongest limit for $E_e = 1$ MeV is from the heating of Leo T, requiring $\tau(\text{DM} \rightarrow e^+ e^-) > 10^{26}$ s for $m_{\text{DM}} = 2$ MeV [40]. Recasting this limit for S yields

$$\tau(S \rightarrow nn) \gtrsim \left(\frac{2 \text{ GeV}}{m_S} \right) 10^{23} \text{ s}, \quad (4.5)$$

because S is roughly 1000 times heavier and therefore the flux of electrons with $E_e = 1$ MeV is 1000 times smaller. The excluded range of \tilde{g} is shown as the pink area in figure 3.

A laboratory limit on $S \rightarrow nn$ arises if we consider SDM with an ambient density n_S in the SNO detector. Phase III of the SNO experiment was equipped with an array of ^3He

⁵A calculation of weak decays of the H-dibaryon is performed in Ref. [4], implicitly assuming the H is weakly bound. Thus the momentum dependence can be estimated and \tilde{g} is not small. They estimate the weight of different types of quark level interactions that govern the decay. For us, these would give a sub-leading source of uncertainty relative to p_q and \tilde{g} .

neutron counters [42] and could observe neutrons produced from $S \rightarrow nn$. Assuming all the neutron events at SNO are due to S decay, we require

$$n_S V \times (1 - e^{-t/\tau}) \times 2 \times \epsilon < N_{\text{obs}}, \quad (4.6)$$

where $V = 904.78 \text{ m}^3$ is the volume of the tank, $\epsilon = 0.182$ is the detector efficiency, and $N_{\text{obs}} \approx 7000$ is the observed number of neutron events during $t = 385.17$ days. To obtain a lower limit on the lifetime τ , we must insert suitable estimations of n_S . There are two possibilities:

- $n_S \sim 0.1/\text{cm}^3$, based on the local DM density of the Galaxy estimated to be $0.2\text{--}0.56 \text{ GeV}/\text{cm}^3$ [53] for $m_S \approx 2 \text{ GeV}$. The corresponding lower limit on the lifetime is $\tau \gtrsim 10^4 \text{ yr}$, which is far weaker than t_{univ} .
- $n_S \sim 10^{14}/\text{cm}^3$, the density of hadronically-interacting DM accumulated in Earth if the effective DM-nucleus cross section is $10^{-30}\text{--}10^{-24} \text{ cm}^2$ [54], denoted the NFM density hereafter. Such strong DM-nuclei cross sections are in fact not ruled out by direct detection experiments and cosmology due to non-perturbative and finite-size effects [18, 19]. With this value of n_S , eq. (4.6) implies $\tau \gtrsim 4.96 \times 10^{18} \text{ yr}$. The corresponding limit on \tilde{g} is shown as the dashed cyan line in Figure 7. However the bound does not apply for an attractive S -nucleus interaction, since then binding of S with nuclei [18, 19] kinematically prevents S decay. We therefore do not show this limit in figure 3.

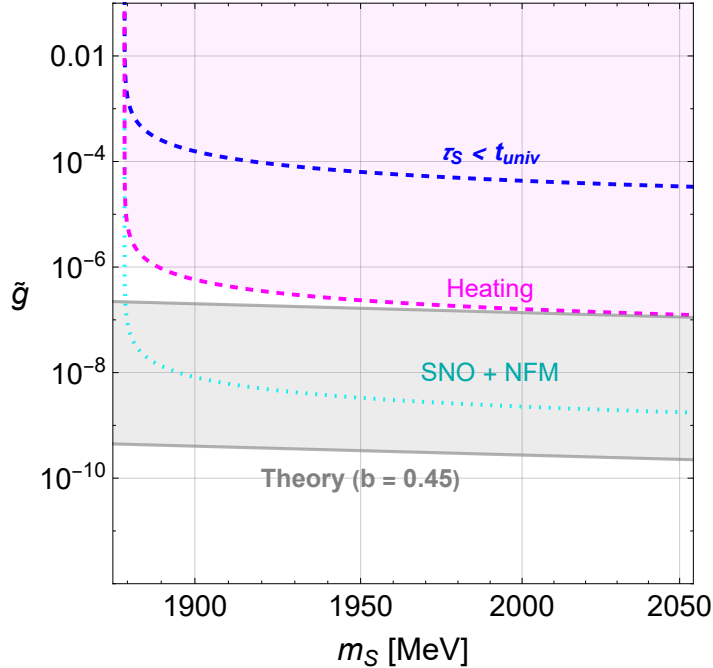


Figure 7: Cyan: the limit on \tilde{g} from the SNO limit on $S \rightarrow nn$, taking $p_q = 100 \text{ MeV}$ and assuming DM is composed of S , and the ambient density of S is the NFM value $n_S \sim 10^{14}/\text{cm}^3$. This limit is only applicable if the DM-baryon interaction is repulsive, hence it is not included in figure 3. Some other limits from Figure 3 are shown for comparison.

4.2 $S \rightarrow De\nu$

Following the analysis of $D \rightarrow Se\nu$ in section 3.1, we can similarly obtain the decay width of $S \rightarrow De\nu$

$$\Gamma = \frac{\tilde{g}^2 G_F^4 p_q^6 \sin^4 \theta_c \cos^2 \theta_c}{40\pi^3 m_D m_S} \int_{m_e}^{m_S - m_D} dE_e \sqrt{E_e^2 - m_e^2} E_e (m_S - m_D - E_e)^2. \quad (4.7)$$

The decay of SDM to deuterons through cosmological history supplies a new source of deuterons in addition to primordial synthesis. Comparing the value of D/H (times 10^{+5}) measured in damped Lyman- α systems 2.53 ± 0.04 [55] and predicted by BBN 2.45 ± 0.1 [56], we conclude $\tau \gtrsim 1.6 \times 10^{15}$ yr. The resulting upper limit on \tilde{g} is shown as the brown curve in figure 3. As a result of the 3-body phase space suppression, it yields a weaker limit on \tilde{g} than requiring $\tau(S \rightarrow nn) > t_{\text{univ}}$, even though the lower limit on lifetime is five orders of magnitude longer than t_{univ} .

4.3 $S \rightarrow n\Lambda$

If $m_S > 2054.47$ MeV, singly-weak decays of S such as $S \rightarrow N\Lambda$ are permitted. This is the mass range initially envisaged for the H-dibaryon [3], where the singly-weak-interaction lifetimes lead to totally different phenomenology and the dibaryon is not a dark matter candidate. For notational convenience, we continue to call the particle S .

Among a number of possible decay channels, we only consider $S \rightarrow n\Lambda$ because of its simple phase space structure. The process can be described by the effective Lagrangian

$$\mathcal{L} \supset \frac{\tilde{g}}{\sqrt{40}} \bar{\psi}_\Lambda (g + ig_5 \gamma^5) \psi_n^c \phi_S. \quad (4.8)$$

Similar to our discussion of $S \rightarrow nn$, we take $g_5 = 0$ and estimate g by the amplitude of the quark diagram in the right panel of figure 6

$$g^2 \simeq G_F^2 p_q^4 \sin^2 \theta_c. \quad (4.9)$$

The decay rate is then given by

$$\Gamma = \frac{\tilde{g}^2 G_F^2 p_q^4 \sin^2 \theta_c}{320\pi} \frac{m_S^2 - 4m_n m_\Lambda}{m_S} \sqrt{\frac{(m_S^2 + m_n^2 - m_\Lambda^2)^2}{m_S^4} - \frac{4m_n^2}{m_S^2}}. \quad (4.10)$$

Not surprisingly, much smaller \tilde{g} is needed in order for SDM to be stable enough once $S \rightarrow n\Lambda$ is allowed. The condition $\tau \gtrsim t_{\text{univ}}$ can only be met in this mass range for unreasonably low \tilde{g} , as indicated by the lower part of the blue region in figure 3. We also calculate the Leo T heating limit, only considering the heating due to electrons from neutron β -decay. The result is shown by the lower part of the pink curve in figure 3. We note that decay products of Λ baryons would also deposit energies to Leo T, making this limit conservative.

5 Laboratory limits on S production

The H-dibaryon, a $uuddss$ state with a ~ 80 MeV binding energy was initially proposed in [3] and lead to many experimental efforts to find it. To date, all experimental searches [6–9, 57–61] for the H-dibaryon report a null finding. These experiments, as reviewed in [1], either require H-dibaryons to decay to certain final states and therefore must be heavy enough,

or the breakup amplitude of H-dibaryons into two Λ 's (the analogue of \tilde{g}) is $\mathcal{O}(1)$. These assumptions make the experimental results not address the question of whether a deeply bound configuration of $uuddss$ quarks with a small \tilde{g} may exist. Below we review a few representative experiments, and recast their results as upper bounds on \tilde{g} .

5.1 Doubly-strange hypernuclei

Hypernuclei that contain two Λ 's have been created in the laboratory [6–9]. The double- Λ hypernucleus is observed to decay weakly to a single- Λ hypernucleus which subsequently decays weakly to ordinary nuclei. The lifetime has not been precisely measured, but is assumed to be the typical weak-interaction lifetime $\sim 10^{-10}$ s [6].

The binding energy of two Λ 's in the nucleus is measured to be $B_{\Lambda\Lambda} \approx 7$ MeV [8]. Based on the observed decay pattern of hypernuclei, an H-dibaryon lighter than $2m_\Lambda - B_{\Lambda\Lambda} \approx 2224$ MeV is determined to be excluded because the formation of $\Lambda\Lambda \rightarrow H$ with a strong-interaction timescale $\sim 10^{-22}$ s would otherwise occur before the hypernucleus decays.

These constraints are evaded if the formation rate of S is slower than the weak decay rate of hypernuclei, which is possible if \tilde{g} is small enough. The transition timescale of $A_{\Lambda\Lambda} \rightarrow A_S$ is worked out in ref. [5]. Requiring it to be longer than 10^{-10} s leads to the exclusion region of \tilde{g} shown by the green area in Figures 8 and 3. The mechanism of S formation $\Lambda\Lambda \rightarrow S$ plus additional pions studied in ref. [5] does not apply to masses above 2100 MeV so the excluded region from that analysis ends there, but with further study the hypernuclei limits could be extended to higher mass.

The E836 collaboration at Brookhaven National Lab (BNL) [62] searched for evidence of H dibaryon production in the reaction ${}^3\text{He}(K^-, K^+)Hn$. The sensitivity was independent of the H lifetime and decay modes, and placed a limit about an order of magnitude lower than the theoretical prediction of [63, 64]. However since the theoretical calculation assumed the H is quite extended, and moreover ignored the short-distance repulsion of two nucleons, the effective value of \tilde{g} underlying the rate prediction was $\tilde{g} \sim \mathcal{O}(1)$. Thus the limit on \tilde{g} from E836 is weaker than from the others we discuss.

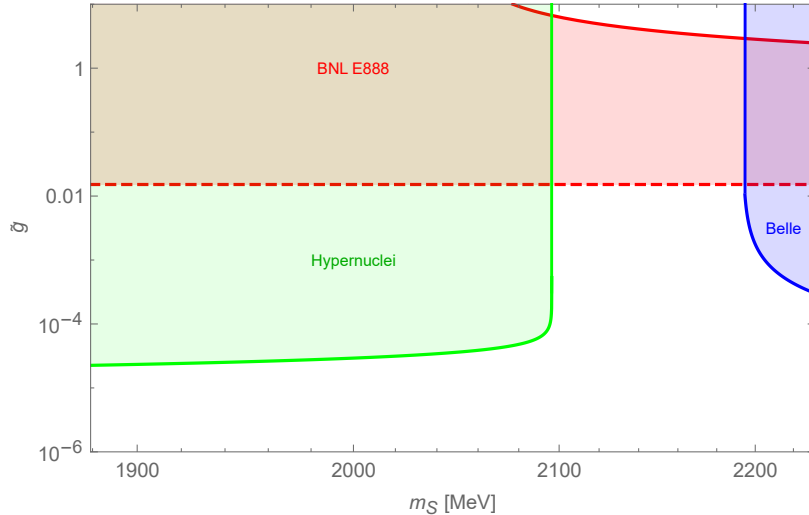


Figure 8: Sensitivity of laboratory H-dibaryon searches to \tilde{g} .

5.2 Diffractive dissociation

Brookhaven E888 searched for neutral long-lived H-dibaryons [60]. The experiment assumes H-dibaryons exist in the neutral beam produced by 24.1 GeV proton-Pt collisions, and a scintillator is placed at a distance of 10^{-8} s downstream of the Pt target. The reaction of interest is the diffractive dissociation of an H-dibaryon into two Λ 's by the scintillator, which are detected by the Λ decay product to $p\pi^-$

$$H + A \rightarrow \Lambda\Lambda A \rightarrow p\pi^- p\pi^- A. \quad (5.1)$$

Similar signals can be triggered by neutrons

$$\begin{aligned} n + A &\rightarrow \Lambda\Lambda X \rightarrow p\pi^- p\pi^- X, \\ n + A &\rightarrow \Lambda K_S X \rightarrow p\pi^- \pi^+ \pi^- X. \end{aligned} \quad (5.2)$$

A 90% confidence level upper bound on the product of σ_S and $\sigma_{\Lambda\Lambda}$, the diffractive dissociation cross section of the H , is placed at [1, 60]

$$\left. \frac{d\sigma_H}{d\Omega} \right|_{65 \text{ mr}} \frac{\sigma_{\Lambda\Lambda}}{0.5 \text{ mb}} < 2.3 \times 10^{-4} \left. \frac{d\sigma_n}{d\Omega} \right|_{65 \text{ mr}} \frac{\sigma_{\Lambda K_S}}{5.9 \mu\text{b}}, \quad (5.3)$$

where σ_n is the production cross section of neutrons, and $\sigma_{\Lambda\Lambda}$ and $\sigma_{\Lambda K_S}$ are the corresponding diffractive dissociation cross sections of H and n respectively. Translating this bound to an exact upper limit on \tilde{g} requires a detailed calculation of σ_S and $\sigma_{\Lambda\Lambda}$ as a function of \tilde{g} . At this point, we only employ a naive estimation $\sigma_S \approx \sigma_n \tilde{g}^2$ so eq. (5.3) implies $\tilde{g} \lesssim 1.5 \times 10^{-2}$, shown by the dashed red line in figure 8. A caveat is that, if \tilde{g} is large enough so that the lifetime of S is shorter than 10^{-8} s, the S would decay before entering the scintillator. This boundary is shown by the solid red line in figure 8.

5.3 Upsilon decay

The Υ decays dominantly into three gluons, and can subsequently source $qqqqqq + \bar{q}\bar{q}\bar{q}\bar{q}\bar{q}\bar{q}$ final states. It is possible that the $6q$ (or $6\bar{q}$) state forms an S (or \bar{S}) if their quantum numbers are identical to the S (\bar{S}). The formation rate of S from Υ decay is thus independent of \tilde{g} , and electron-positron colliders such as BaBar and Belle can provide discovery opportunities. However, the probability that the six quarks are singlet under color-spin-flavor is statistically penalized. Ref. [1] estimates that the inclusive branching ratio to be $BR(\Upsilon \rightarrow SX) \approx 2.7 \times 10^{-7}$.

An inclusive search for the H-dibaryon from Υ decay was performed by Belle [57]. The signal being sought was the decay of H into $\Lambda p\pi^-$. An upper bound on

$$BR(\Upsilon \rightarrow HX) \times BR(H \rightarrow \Lambda p\pi) \lesssim 10^{-7} \quad (5.4)$$

was obtained, applicable if $m_S > m_p + m_\Lambda + m_\pi = 2193$ MeV.

To recast the Belle limit for S , we must take into account that the S could be much longer-lived than H due to a small \tilde{g} . This leads to the possibility that S could escape the detector before decaying to $\Lambda p\pi$. Thus, we re-interpret eq. (5.4) by

$$BR(\Upsilon \rightarrow SX) \times BR(S \rightarrow \Lambda p\pi) \times \frac{L}{l(S \rightarrow \Lambda p\pi)} \lesssim 10^{-7}, \quad (5.5)$$

where $L \approx 3$ m is the detector size and $l(S \rightarrow \Lambda p \pi) = \beta \gamma c \times \tau(S \rightarrow \Lambda p \pi)$ is the decay length. To proceed, we take $BR(\Upsilon \rightarrow SX) = 2.7 \times 10^{-7}$, and estimate $BR(S \rightarrow \Lambda p \pi)$ by the 3-body phase space suppression factor $\Gamma(S \rightarrow \Lambda p \pi)/\Gamma(S \rightarrow n \Lambda) \sim 1/(8\pi^2)$. The lifetime of $S \rightarrow \Lambda p \pi$ is a function of m_S and \tilde{g} ; details are given in appendix D. The blue region in figure 8 shows the exclusion range of \tilde{g} from the Belle experiment, applicable for $m_S > m_p + m_\Lambda + m_\pi = 2193$ MeV. Unfortunately, this mass range is not of interest for SDM.

5.4 Cooling of SN1987a

In addition to the laboratory constraints on \tilde{g} discussed above and in figure 3, a limit from the cooling time of SN1987a was obtained by McDermott et al [37].⁶ We adapt their calculation and find the maximum allowed value of \tilde{g} such that the cooling time of SN1987a is not shorter than $\mathcal{O}(10)$ s. This is shown by the red line in figure 3. Details are given in Appendix C.

6 Isgur-Karl model of \tilde{g}

In this section, we derive the gray band in figure 3 which represents the theoretical modeling of \tilde{g} , following the methodology of Ref. [5] (FZ03 below) and [18]. Effectively, \tilde{g} is the Yukawa coupling of the flavor-conserving SBB' vertex which naively could be expected to be $\mathcal{O}(1)$ since the interaction is hadronic. However FZ03 argued that this naive intuition is incorrect because \tilde{g} is the transition amplitude between the states: $\tilde{g} \equiv |\langle S | H_{\text{QCD}} | BB' \rangle|$. FZ03 pointed out that \tilde{g} is suppressed on account of several factors: i) the well-known strong short-distance repulsion between two baryons due to Fermi statistics, ii) the relatively small spatial size of the S , and iii) the necessity that all 6 quarks fluctuate between rather orthogonal initial and final states. Below we first summarize the FZ03 calculation, then point out an additional effect due to the tunneling-amplitude (analogous to the Gamov suppression factor in nucleosynthesis) which was not included by FZ03.

In the leading approximation of ignoring interactions, setting $H_{\text{QCD}} \rightarrow 1$, \tilde{g} is just the overlap of the spatial wavefunctions of S and BB' . The overlap was evaluated in FZ03, taking the wavefunctions of the quarks in the baryons and S to be solutions of harmonic oscillator potentials, which are entirely specified by their root mean square radii, r_B and r_S . This is a simple extension of the Isgur-Karl model of baryons [66]. The overlap also depends on the relative wavefunction of the baryons, $u(a)$, where a is the separation between the centers of mass of the two baryons. The general expression for the overlap is given in FZ03

$$|\mathcal{M}| = \left(\frac{3}{2\pi r_S^2} \right)^{3/4} \left(\frac{2r_S/r_B}{1 + (r_S/r_B)^2} \right)^6 \times \int_0^\infty d^3a \frac{u(a)}{a} \exp\left(-\frac{3}{4} \frac{a^2}{r_S^2}\right). \quad (6.1)$$

A practical choice for $u(a)$ is the Brueckner-Bethe-Goldstone (BBG) wavefunction, which describes the state of two asymptotically free particles in a repulsive short distance potential having a hardcore radius r_c .⁷ In the BBG approximation, the baryons are free except for an infinite potential barrier between them below a hardcore radius r_c . Thus r_c sets the lower bound on the separation of the baryons' centers of mass, a . The short distance behavior of

⁶See however [65], where the $\mathcal{O}(10)$ s cooling time of SN1987a is challenged. The SN1987a constraint on S may therefore need to be revised.

⁷To describe the transition within a nucleus, as for the hypernuclear experiments, one should use the relative wavefunction of two nucleons in a nucleus. This is discussed in FZ03, where it is found that the transition amplitude is only weakly sensitive to the size of the nucleus for larger nuclei. This justifies our approximating the transition amplitude in all cases by the single parameter \tilde{g} , in our phenomenological discussions above.

the inter-baryon potential is crucial for determining \tilde{g} and has often been incorrectly modeled in the literature on \tilde{g} , so we devote section 7.1 to a review of present knowledge of r_c . For our calculations we use the BBG wavefunction with the conservative choice $r_c = 0.4$ fm.

In order to evaluate Eq. (6.1) we require an estimate of r_S . Due to the non-coupling of S to pions and other flavor-octet pseudoscalar mesons (except through an off-diagonal transition to heavier flavor-octet di-baryons), r_S can be expected to be considerably smaller than r_p . An empirical radius-mass relationship based on the Compton wavelengths of a hadron and the lightest meson it couples to is [13]

$$r(m) = \frac{1}{m} + \frac{b}{m'}, \quad (6.2)$$

where b is a non-negative coefficient, and m' is the mass of the lightest meson that strongly couples to the baryon. Fitting the charge radius of protons $r_p = 0.87$ fm with $m' = m_\pi = 135$ MeV gives $b = 0.45$. The second term in eq. (6.2) accounts for the fact that the pion cloud makes a significant contribution to r_p . The relationship eq. (6.2) may be generalized to other hadrons with b varying from 0 to 0.45, depending on its coupling to mesons. The S is expected to couple most strongly to the flavor-singlet combination of ω and ϕ vector mesons [13] with $m' \approx 1000$ MeV, giving $r_S \lesssim 0.2$ fm.⁸ Using eq. (6.2), we can then recast the expression eq. (6.1) into a function $\mathcal{M}(m_S)$; for our estimates we conservatively adopt $b = 0.45$.

In addition to the wavefunction overlap, an additional factor may suppress \tilde{g} , namely the tunneling of the 6-quark configuration between BB and S . Overall, \tilde{g} is given by

$$\tilde{g} = e^{-\mathcal{S}} \times |\mathcal{M}|. \quad (6.3)$$

The tunneling action \mathcal{S} can be estimated as follows [18]. The characteristic momentum p_q of each constituent quark varies from the QCD scale, ~ 100 MeV, to the constituent quark mass scale ($\gtrsim 340$ MeV); the timescale Δt for the transition is roughly the typical hadronic length-scale ($\mathcal{O}(1)$ fm) divided by the speed of light. Summing the action $\mathcal{S} \approx p_q \Delta t$ over six quarks gives $e^{-\mathcal{S}} = 10^{-4} - 0.05$. The gray band in figure 3 shows the range of \tilde{g} , corresponding to $r_c = 0.4$ fm and $b = 0.45$, with the width of the band set by the range of estimated tunneling suppression factor $e^{-\mathcal{S}} = 10^{-4} - 0.05$. Changing b to a smaller value would decrease r_S and further suppress \tilde{g} . For a conservative choice, we take $b = 0.45$ and only show \tilde{g} with $b = 0.45$ in figure 3.

We stress that a more detailed estimate of the tunneling suppression of \tilde{g} is warranted. For example, if the S is made of three scalar di-quarks $S = \epsilon_{\alpha\beta\gamma}(ud)^\alpha(us)^\beta(ds)^\gamma$ [14, 32], the transition $S \rightarrow BB$ must unbind at least two of the three di-quarks to rearrange the system into two color-singlet baryons. This would imply a more highly suppressed tunneling action if the di-quark binding is as strong as some estimates indicate [14, 32].

7 Critics review

In this section, we review existing literature where negative arguments against S as a stable hadron or S as DM were presented. We also compile from existing literature the potential solutions to those negative arguments. As these arguments are not completely conclusive at this stage, discovering or excluding S is still an open and continuing quest.

⁸In [67], we use an independent method based on QCD sum rules which agrees with $r_S \ll r_p$.

7.1 Short-distance repulsion between baryons

A recurring source of divergence in conclusions about present constraints on the S arises from treatment of the short distance potential between baryons, which strongly influences the wavefunction overlap calculation of \tilde{g} discussed in the previous section. The existence of a short distance repulsion between baryons was one of the first properties of hadronic interactions to be observed. It is responsible for the fact that nuclear radii scale as $A^{1/3}$ to good accuracy, and for the approximate incompressibility of nuclear matter. We now understand that this so called hard-core repulsion is due to Fermi statistics at the quark level. In the widely-used Brueckner-Bethe-Goldstone (BBG) wavefunction, the nucleons are taken to be free when their centers of mass are separated by more than the hard-core radius r_c , within which the potential is infinite. The value of r_c is constrained by nucleon-nucleon phase shifts; the fits indicate $r_c \approx 0.4$ fm, with $r_c < 0.3$ fm or $r_c > 0.5$ fm being experimentally disfavored [68]. Many other well-known NN potentials also include a hard core; for a recent review see [69]. These potentials are constructed based on measurements of phase shift and NN scattering. For example, the Hamada-Johnston potential [70] has a hard core radius 0.343 fm and the Reid potential [71] has a hard core radius near 0.4 fm. The potential between two baryons can also be found using lattice QCD. Figure 1 of [10] shows that below $a = 0.6$ fm (where a is the separation) the $\Lambda\Lambda$ potential is repulsive, with the repulsion increasing very rapidly at smaller separation to exceed 125 MeV below $a = 0.4$ fm where the plot cuts off. Thus the hard-core BBG approximation with no repulsion at distances larger than $r_c = 0.4$ fm gives a conservative estimate of the suppression in \tilde{g} due to the wavefunction overlap. Calculations of the wavefunction overlap not taking into account the hard-core repulsion, such as in [14, 37] which computed \tilde{g} based on the Isgur-Karl model following [5] but ignored hardcore repulsion, grossly overestimate \tilde{g} .

7.2 S and oxygen stability

Ref. [14] computed \tilde{g} following the methodology of [5] (described in Sec. 6) but used a nucleon-nucleon (NN) wavefunction interpolated from [72]. However the focus of Ref. [72] is the form of the wavefunction at large distances and their wavefunction was not constrained to have the known hard-core at short distances. The authors of [14], by comparing their value of \tilde{g} calculated without taking the hard core into account, to the estimated limits on \tilde{g} from the oxygen stability in the SuperK detector given in [5], concluded that S is ruled out for $m_S \lesssim 1860$ MeV, the mass below which two nucleons in an oxygen atom can convert to an S . It is noteworthy that Ref. [14] also calculated \tilde{g} using the BBG wavefunction with a hardcore radius 0.5 fm and found \tilde{g} can be suppressed down to 10^{-10} agreeing with [5].

The determination of \tilde{g} from spatial wavefunctions is extremely sensitive to whether the hard core is included in the NN wavefunction as discussed in Sec. 7.1. Studies which do not take the hard core into account therefore obtain inaccurate (overly strong) constraints on the allowed properties of the S .

7.3 S and neutron stars

The impact of S on the cooling of SN1987a is studied in [37], where it was required that in the hot and dense baryonic environment of the proto-neutron star, the timescale of the reaction $\Lambda\Lambda \leftrightarrow S\gamma$ must be longer than the observed cooling time $\mathcal{O}(10)$ s. (In appendix C, we recast their calculation to obtain the supernova cooling upper limits on \tilde{g} .) The authors of [37] then presented two arguments against the existence of S . (i) The authors computed \tilde{g} following [5]

in the Isgur-Karl model using a Brueckner-Bethe-Goldstone NN wavefunction without a hard core, and found that the estimated value of \tilde{g} is too large to be compatible with an $\mathcal{O}(10)$ s cooling time. (ii) It was also qualitatively argued that the presence of S inside neutron stars would soften the equation of state, and thus be severely challenged by the existence of neutron stars with masses above two solar masses. Argument (i) is obviated by including a hard core in the NN wavefunction, as discussed in Sec. 7.1. Argument (ii) was addressed in ref. [73], which showed that quark de-confinement in the center of massive neutron stars gives good agreement with neutron star observations and is favored phenomenologically with or without the existence of a deeply bound S .

7.4 Relic abundance of S

As discussed in Sec. 1, Ref. [15] studied the thermal evolution of S and reported that the relic density of S today is too small to make up a significant portion of the DM, unless (i) $m_S \lesssim 1.2$ GeV or (ii) the breakup cross section of $XS \rightarrow BB'$ is much smaller than QCD-scale cross sections. The possibility (i) is not feasible as an S lighter than 1.2 GeV would destabilize nuclei by converting nucleons to S and kaons. The possibility (ii) was studied in [13], where the condition $\tilde{g} \lesssim 2 \times 10^{-6}$ was derived in order for S not to thermalize in the early Universe. This is detailed in appendix A.

7.5 Direct detection, CMB and S DM

The direct detection, astrophysical and CMB signals of S DM (assuming S is the entirety of DM) were studied in depth in [19]. It was shown that due to a combination of overburden, non-perturbative phenomenon and extended size of nuclei, for GeV-scale DM a DM-nucleon cross section $\lesssim 10^{-26}$ cm² is not excluded by current limits. A general difficulty for direct detection of DM in the $\mathcal{O}(\text{GeV})$ mass range, is that DM with typical virial velocity $v \sim 10^{-3}c$ often does not carry enough energy to pass trigger threshold, even if it does scatter in the detector. An ingenious observation is that there should be a population of DM with up to \approx GeV kinetic energy, as a result of upscattering by cosmic rays [74]. The recent study [75] places limits on "CRDM" lying in the sweet spot of having small enough cross-section to reach the Xe1T detector in the Gran Sasso National Lab without too much energy loss in the overburden. Using a perturbative approximation, [75] concluded that the S could be excluded. However for the coupling and mass range of interest for the S , non-perturbative effects are strong and lead to a short energy-loss length, such that S CRDM do not in general reach Xe1T with sufficient energy to be detected; for details see [76].

8 Summary

To conclude, we have derived observational constraints on \tilde{g} , the sexaquark dissociation amplitude into two baryons, as a function of its mass. Our new, most constraining limit on \tilde{g} comes from SNO limits on e^+ appearance, applicable if S is lighter than deuterium by more than 5.5 MeV, the SNO threshold for positron detection. This significantly improves the previous best limit obtained in [5] based on oxygen decay in the SuperK detector. Comparing to theoretical estimates for \tilde{g} , we conclude that $m_S < 1.80$ GeV is strongly disfavored based on the stability of deuterium. For $m_S \gtrsim 2m_N \approx 1.88$ GeV, the strongest limits on \tilde{g} are from supernovae and hypernuclei experiments, with the latter requiring $\tilde{g} \lesssim 10^{-5} - 10^{-6}$ depending on the value of m_S . We also reviewed the existing laboratory searches for the H-dibaryon and concluded that the best limits exclude $\tilde{g} \gtrsim 10^{-5}$. We set additional limits on \tilde{g} that are

applicable if the S makes up all, or in some cases just part of, the dark matter. In particular, we obtain new, much stronger limits for $m_S \gtrsim 2m_N \approx 1.88$ GeV, required to avoid the decay of S to baryons overheating astrophysical environments. These are the most constraining limits for $m_S \gtrsim 1.9$ GeV, unless S 's constitute $\approx 10\%$ or less of the dark matter.

Acknowledgments

We thank Hartmut Wittig for comments on lattice QCD calculations. ZW thanks Aksel Hallin and Tony Noble for discussions on the sensitivity of the SNO detector to positrons, and Xuyao Hu, Di Liu, Sam McDermott, Marco Muzio, Po-Jen Wang and Xingchen Xu for helpful conversations. Feynman diagrams in this paper are generated by a Feynman diagram maker developed by Aidan Randle-Conde. The research of GRF was supported by NSF-PHY-2013199 and the Simons Foundation. The work of ZW was supported in part by NSF-PHY-2013199, MacCracken Fellowship and James Arthur Graduate Fellowship.

A Non-thermalization of S in the early Universe

In this appendix we calculate the range of \tilde{g} so that S does not chemically thermalize with baryons in the hot hadronic early Universe. We consider processes that convert S to two-baryon states, $K^+S \rightarrow p\Lambda$, $\pi^\pm S \rightarrow \Sigma^\pm\Lambda$, $\gamma S \rightarrow \Lambda\Lambda$ and $\pi\pi S \rightarrow \Lambda\Lambda$. Note that $\pi S \rightarrow \Lambda\Lambda$ is forbidden by isospin conservation. The amplitudes of the first two reactions can be found in [13], that of the third in [37], and we scale the rate of $\pi\pi S \rightarrow \Lambda\Lambda$ given in [15] by $\tilde{g}^2/40$. We then follow the procedure in [77] to calculate thermal cross sections. Figure 9 shows the

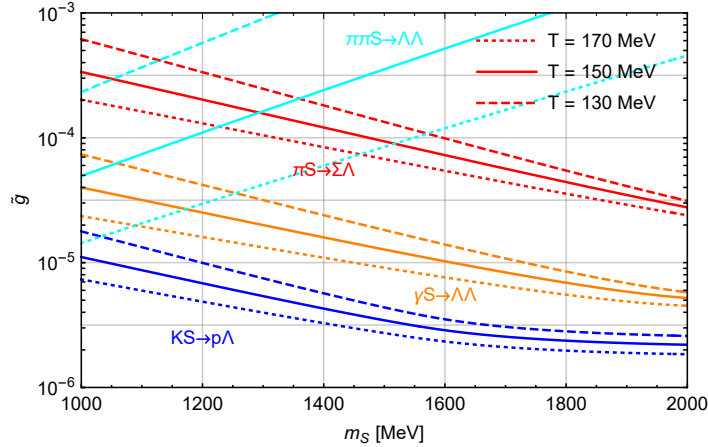


Figure 9: Maximum values of \tilde{g} for which $n_X \langle \sigma v \rangle_{XS \rightarrow BB} < H$. Dashed, solid and dotted lines assume $T = 130, 150$ and 170 MeV.

maximum values of \tilde{g} for which $n_X \langle \sigma v \rangle_{XS \rightarrow BB} < H$. In our calculation, we have assumed that the transition from the quark-gluon plasma phase to the hadronic phase takes place abruptly at a temperature T , which we vary from 130 to 170 MeV. We also find that the dominant breakup process is $KS \rightarrow p\Lambda$, despite n_K being smaller than n_π and n_γ . The suppression of $\pi S \rightarrow \Sigma\Lambda$ arises from a flavor SU(3) cancellation [13], and $\gamma S \rightarrow \Lambda\Lambda$ from the magnetic moment of Λ [37]. For $\tilde{g} \lesssim 2 \times 10^{-6}$, all of these reactions are slower than the Hubble rate.

B Color-spin-flavor wavefunction projection

The normalization factor $\tilde{g}/\sqrt{40}$ in eq. (2.1) is chosen as follows. The total transition amplitude between an S and a two-baryon state, $\langle S|BB'\rangle$, consists of two contributions. Firstly, we denote the dynamical amplitude of six quarks transitioning between S and two baryons by

$$\tilde{g} = \langle S|H_{\text{QCD}}|BB'\rangle. \quad (\text{B.1})$$

Secondly, the projection of color-spin-flavor (CSF) wavefunctions between $|S\rangle$ and $|BB'\rangle$ involves Clebsch-Gordan decomposition. The S is a singlet under color SU(3), spin SU(2) and flavor SU(3) separately, with its CSF wavefunction given by [17]

$$|S\rangle = \frac{1}{16\sqrt{3}}(\epsilon_{\alpha\mu\rho}\epsilon_{\beta\nu\sigma}\epsilon_{im}\epsilon_{jk}\epsilon_{ln} - \epsilon_{\alpha\beta\rho}\epsilon_{\mu\nu\sigma}\epsilon_{im}\epsilon_{jl}\epsilon_{kn})u_{\alpha,i}^\dagger u_{\beta,j}^\dagger d_{\mu,k}^\dagger d_{\nu,l}^\dagger s_{\rho,m}^\dagger s_{\sigma,n}^\dagger |\Omega\rangle, \quad (\text{B.2})$$

where Greek (Latin) letters indicate color (spin) indices, $u^\dagger, d^\dagger, s^\dagger$ are the field operators for up, down and strange quarks, and $|\Omega\rangle$ is the QCD vacuum. Similar expressions for baryons can be found in e.g. [78]. Equivalently, the representations of S and baryons under CSF can be depicted by the Young diagrams listed in table 1. The eight di-baryon configurations containing a flavor-singlet component are $\Lambda\Lambda, \Sigma^0\Sigma^0, \Sigma^+\Sigma^-, \Sigma^-\Sigma^+, p\Xi^-, \Xi^-p, n\Xi^0$ and Ξ^0n [79]. Projecting the CSF wavefunctions of di-baryons to S leads to a factor of $\pm 1/\sqrt{40}$. Thus, the total transition amplitudes are [17]

$$\begin{aligned} \langle S|\Lambda\Lambda\rangle &= \langle S|\Sigma^0\Sigma^0\rangle = -\langle S|\Sigma^+\Sigma^-\rangle = -\langle S|\Sigma^-\Sigma^+\rangle = \langle S|p\Xi^-\rangle \\ &= \langle S|\Xi^-p\rangle = -\langle S|n\Xi^0\rangle = -\langle S|\Xi^0n\rangle = \frac{\tilde{g}}{\sqrt{40}}. \end{aligned} \quad (\text{B.3})$$

	SU(3) color	SU(3) flavor	SU(2) spin
S	$\begin{array}{ c c } \hline \square & \square \\ \hline \end{array} = \mathbf{1}$	$\begin{array}{ c c } \hline \square & \square \\ \hline \end{array} = \mathbf{1}$	$\begin{array}{ c c } \hline \square & \square \\ \hline \end{array} = \mathbf{1}$
B	$\begin{array}{ c } \hline \square \\ \hline \end{array} = \mathbf{1}$	$\begin{array}{ c c } \hline \square & \square \\ \hline \end{array} = \mathbf{8}$	$\begin{array}{ c } \hline \square \\ \hline \end{array} = \mathbf{2}$

Table 1: Representations of S and octet baryons under CSF.

C Cooling of SN1987a

In this appendix, we recast the calculation in ref. [37] to constrain \tilde{g} as a function of m_S . The hot and dense environment in proto-neutron stars can spontaneously create an abundant amount of hyperons. If the reaction rate of $\Lambda\Lambda \rightarrow S\gamma$ is rapid enough, S would be brought into thermal equilibrium with baryons and hyperons in the star. The timescale needed for S to equilibrate is estimated by ref. [37] to be

$$t_S = \text{s} \frac{4 \times 10^{-34} \text{cm}^3/\text{s}}{\langle \sigma_{\Lambda\Lambda \rightarrow S\gamma} v \rangle} \left(1 + \frac{2 \times 10^{-32} \text{cm}^3/\text{s}}{\langle \sigma_{NN \rightarrow N\Lambda} v \rangle} \right)^2, \quad (\text{C.1})$$

with

$$\langle \sigma_{NN \rightarrow N\Lambda} v \rangle = 3 \times 10^{-30} \text{cm}^3/\text{s}, \quad \langle \sigma_{\Lambda\Lambda \rightarrow S\gamma} v \rangle = 3 \times 10^{-23} \frac{g_{\Lambda S}^2 (2m_\Lambda - m_S)}{176.9 \text{MeV}} \text{cm}^3/\text{s}. \quad (\text{C.2})$$

Note that the coupling $g_{\Lambda S}$ in their notation is related to \tilde{g} by $\tilde{g} = \sqrt{40}g_{\Lambda S}$. Observations of neutrinos from SN1987a suggests a core-collapse supernovae from a proto-neutron star with a cooling time ~ 10 s [80] (see, however, ref. [65] for an alternate model). Requiring $t_S \gtrsim 10$ s implies the upper limit on \tilde{g} shown as the red line in Figure 3.

D $S \rightarrow \Lambda p \pi$

Figure 10 shows the effective Feynman diagram of the decay $S \rightarrow \Lambda p \pi$, and we construct the

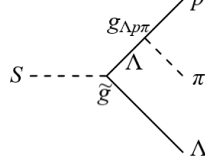


Figure 10: Feynman diagram for $S \rightarrow \Lambda p \pi$.

following meson-baryon Lagrangian

$$\mathcal{L} \supset g_{\Lambda p \pi} \bar{\psi}_{\Lambda} (A + iB\gamma^5) \psi_p \phi_{\pi} + \frac{i\tilde{g}}{\sqrt{40}} \bar{\psi}_{\Lambda} \gamma^5 \psi_{\Lambda}^c \phi_S. \quad (\text{D.1})$$

The coefficients $A = 1.05$ and $B = -7.15$ determine the strength of parity-violating and parity-conserving amplitudes of $\Lambda \rightarrow p \pi$ [81]. To fix the value of $g_{\Lambda p \pi}$, we compute the decay rate

$$\Gamma(\Lambda \rightarrow p \pi) = \frac{g_{\Lambda p \pi}^2}{8\pi} [A^2(E_p + m_p) + B^2(E_p - m_p)] \sqrt{\frac{(m_{\Lambda}^2 + m_p^2 - m_{\pi}^2)^2}{m_{\Lambda}^4} - \frac{4m_p^2}{m_{\Lambda}^2}}, \quad (\text{D.2})$$

where $E_p = (m_{\Lambda}^2 + m_p^2 - m_{\pi}^2)/(2m_{\Lambda})$ is the energy of the proton in the rest frame of Λ . By matching with the measured Λ lifetime 2.6×10^{-10} s [82], we find $g_{\Lambda p \pi} = 3.87 \times 10^{-7}$. Then, the decay rate of $S \rightarrow \Lambda p \pi$ can be evaluated by the integral

$$\Gamma(S \rightarrow \Lambda p \pi) = \frac{1}{2m_S} \int d\Phi_3 \langle |\mathcal{A}|^2 \rangle, \quad (\text{D.3})$$

where Φ_3 is the 3-body phase space factor, and for simplicity we approximate $\langle |\mathcal{A}|^2 \rangle$ by a constant $\langle |\mathcal{A}|^2 \rangle \simeq \tilde{g}^2 g_{\Lambda p \pi}^2 / 40$.

References

- [1] G. R. Farrar, *Stable Sexaquark*, [1708.08951](#).
- [2] G. R. Farrar, *A Stable Sexaquark: Overview and Discovery Strategies*, [2201.01334](#).
- [3] R. L. Jaffe, *Perhaps a Stable Dihyperon*, *Phys. Rev. Lett.* **38** (1977) 195.
- [4] J. F. Donoghue, E. Golowich and B. R. Holstein, *Weak decays of the h dibaryon*, *Phys. Rev. D* **34** (1986) 3434.
- [5] G. R. Farrar and G. Zaharijas, *Nuclear and nucleon transitions of the H dibaryon*, *Phys. Rev. D* **70** (2004) 014008 [[hep-ph/0308137](#)].

- [6] S. Aoki et al., *Direct observation of sequential weak decay of a double hypernucleus*, *Prog. Theor. Phys.* **85** (1991) 1287.
- [7] J. K. Ahn et al., *Production of $(\Lambda\Lambda)H$ -4 hypernuclei*, *Phys. Rev. Lett.* **87** (2001) 132504.
- [8] H. Takahashi et al., *Observation of a $(\Lambda\Lambda)He$ -6 double hypernucleus*, *Phys. Rev. Lett.* **87** (2001) 212502.
- [9] KEK-E176, J-PARC-E07 collaboration, *Double-Lambda hypernuclei via the Ξ -hyperon capture at rest reaction in a hybrid emulsion*, *Nucl. Phys.* **A835** (2010) 207.
- [10] HAL QCD collaboration, *$\Lambda\Lambda$ and $N\Xi$ interactions from lattice QCD near the physical point*, *Nucl. Phys. A* **998** (2020) 121737 [[1912.08630](#)].
- [11] J. R. Green, A. D. Hanlon, P. M. Junnarkar and H. Wittig, *Weakly bound h dibaryon from $su(3)$ -flavor-symmetric qcd*, *Physical Review Letters* **127** (2021) .
- [12] ALICE collaboration, *Study of the Λ - Λ interaction with femtoscopy correlations in pp and p-Pb collisions at the LHC*, *Phys. Lett. B* **797** (2019) 134822 [[1905.07209](#)].
- [13] G. R. Farrar, *A precision test of the nature of dark matter and a probe of the qcd phase transition*, [1805.03723](#).
- [14] C. Gross, A. Polosa, A. Strumia, A. Urbano and W. Xue, *Dark Matter in the Standard Model?*, *Phys. Rev.* **D98** (2018) 063005 [[1803.10242](#)].
- [15] E. W. Kolb and M. S. Turner, *Dibaryons cannot be the dark matter*, *Phys. Rev.* **D99** (2019) 063519 [[1809.06003](#)].
- [16] N. N. Achasov, J. V. Bennett, A. V. Kiselev, E. A. Kozyrev and G. N. Shestakov, *Evidence of the four-quark nature of $f_0(980)$ and $f_0(500)$* , *Phys. Rev. D* **103** (2021) 014010 [[2009.04191](#)].
- [17] G. R. Farrar and N. Wintergerst, *Wave Function of the Sexaquark or Compact H -dibaryon (In preparation)*, 2023.
- [18] G. R. Farrar, Z. Wang and X. Xu, *Dark Matter Particle in QCD*, [2007.10378](#).
- [19] X. Xu and G. R. Farrar, *Resonant scattering between dark matter and baryons: Revised direct detection and CMB limits*, *Phys. Rev. D* **107** (2023) 095028 [[2101.00142](#)].
- [20] J. L. Rosner, *$SU(3)$ Breaking and the H Dibaryon*, *Phys. Rev.* **D33** (1986) 2043.
- [21] C. Gignoux, B. Silvestre-Brac and J. M. Richard, *Possibility of Stable Multi - Quark Baryons*, *Phys. Lett.* **B193** (1987) 323.
- [22] C. G. Callan, Jr. and I. R. Klebanov, *Bound State Approach to Strangeness in the Skyrme Model*, *Nucl. Phys.* **B262** (1985) 365.
- [23] U. Straub, Z.-Y. Zhang, K. Brauer, A. Faessler and S. B. Khadkikar, *Binding Energy of the Dihyperon in the Quark Cluster Model*, *Phys. Lett.* **B200** (1988) 241.
- [24] K. Nishikawa, N. Aoki and H. Hyuga, *Hyperons and the H particle in the color dielectric model*, *Nucl. Phys.* **A534** (1991) 573.
- [25] M. Oka and S. Takeuchi, *Instanton Induced Interaction and the Strange Dibaryons*, *Nucl. Phys.* **A524** (1991) 649.
- [26] J. Haidenbauer and U. G. Meissner, *Exotic bound states of two baryons in light of chiral effective field theory*, *Nucl. Phys.* **A881** (2012) 44 [[1111.4069](#)].
- [27] HAL QCD collaboration, *Bound H -dibaryon in Flavor $SU(3)$ Limit of Lattice QCD*, *Phys. Rev. Lett.* **106** (2011) 162002 [[1012.5928](#)].
- [28] NPLQCD collaboration, *Light Nuclei and Hypernuclei from Quantum Chromodynamics in the Limit of $SU(3)$ Flavor Symmetry*, *Phys. Rev.* **D87** (2013) 034506 [[1206.5219](#)].

- [29] N. Kodama, M. Oka and T. Hatsuda, *H dibaryon in the QCD sum rule*, *Nucl. Phys. A* **580** (1994) 445 [[hep-ph/9404221](#)].
- [30] K. Azizi, S. S. Agaev and H. Sundu, *The Scalar Hexaquark uuddss: a Candidate to Dark Matter?*, *J. Phys. G* **47** (2020) 095001 [[1904.09913](#)].
- [31] N. Evans and M. Ward, *Running anomalous dimensions in holographic QCD: From the proton to the sexaquark*, *Phys. Rev. D* **108** (2023) 026018 [[2304.10816](#)].
- [32] F. Buccella, *On the Mass and on the Dynamical Properties of the Sexaquark*, *PoS CORFU2019* (2020) 024.
- [33] D. McKeen, A. E. Nelson, S. Reddy and D. Zhou, *Neutron stars exclude light dark baryons*, *Phys. Rev. Lett.* **121** (2018) 061802 [[1802.08244](#)].
- [34] G. Baym, D. Beck, P. Geltenbort and J. Shelton, *Testing dark decays of baryons in neutron stars*, *Phys. Rev. Lett.* **121** (2018) 061801 [[1802.08282](#)].
- [35] M. Shahrbafe, D. Blaschke, S. Typel, G. R. Farrar and D. E. Alvarez-Castillo, *Sexaquark dilemma in neutron stars and its solution by quark deconfinement*, *Phys. Rev. D* **105** (2022) 103005 [[2202.00652](#)].
- [36] V. Poulin, P. D. Serpico and J. Lesgourgues, *A fresh look at linear cosmological constraints on a decaying dark matter component*, *JCAP* **08** (2016) 036 [[1606.02073](#)].
- [37] S. D. McDermott, S. Reddy and S. Sen, *Deeply bound dibaryon is incompatible with neutron stars and supernovae*, *Phys. Rev. D* **99** (2019) 035013 [[1809.06765](#)].
- [38] T. R. Slatyer and C.-L. Wu, *General Constraints on Dark Matter Decay from the Cosmic Microwave Background*, *Phys. Rev. D* **95** (2017) 023010 [[1610.06933](#)].
- [39] H. Liu, W. Qin, G. W. Ridgway and T. R. Slatyer, *Lyman- α constraints on cosmic heating from dark matter annihilation and decay*, *Phys. Rev. D* **104** (2021) 043514 [[2008.01084](#)].
- [40] D. Wadekar and Z. Wang, *Strong constraints on decay and annihilation of dark matter from heating of gas-rich dwarf galaxies*, *Phys. Rev. D* **106** (2022) 075007 [[2111.08025](#)].
- [41] M. Garcon and J. W. Van Orden, *The Deuteron: Structure and form-factors*, *Adv. Nucl. Phys.* **26** (2001) 293 [[nucl-th/0102049](#)].
- [42] SNO collaboration, *The Sudbury Neutrino Observatory*, *Nucl. Phys. B* **908** (2016) 30 [[1602.02469](#)].
- [43] T. Siebert, R. Diehl, G. Khachatryan, M. G. Krause, F. Guglielmetti, J. Greiner et al., *Gamma-ray spectroscopy of Positron Annihilation in the Milky Way*, *Astron. Astrophys.* **586** (2016) A84 [[1512.00325](#)].
- [44] W. DeRocco and P. W. Graham, *Constraining Primordial Black Hole Abundance with the Galactic 511 keV Line*, *Phys. Rev. Lett.* **123** (2019) 251102 [[1906.07740](#)].
- [45] SUPER-KAMIOKANDE collaboration, *Search for Nucleon and Dinucleon Decays with an Invisible Particle and a Charged Lepton in the Final State at the Super-Kamiokande Experiment*, *Phys. Rev. Lett.* **115** (2015) 121803 [[1508.05530](#)].
- [46] J. Heeck and V. Takhistov, *Inclusive Nucleon Decay Searches as a Frontier of Baryon Number Violation*, *Phys. Rev. D* **101** (2020) 015005 [[1910.07647](#)].
- [47] R. D. Peccei and H. R. Quinn, *CP Conservation in the Presence of Instantons*, *Phys. Rev. Lett.* **38** (1977) 1440.
- [48] S. Dodelson and L. M. Widrow, *Sterile-neutrinos as dark matter*, *Phys. Rev. Lett.* **72** (1994) 17 [[hep-ph/9303287](#)].
- [49] Z. Berezhiani, A. D. Dolgov and I. I. Tkachev, *Reconciling Planck results with low redshift astronomical measurements*, *Phys. Rev. D* **92** (2015) 061303 [[1505.03644](#)].

- [50] K. Enqvist, S. Nadathur, T. Sekiguchi and T. Takahashi, *Decaying dark matter and the tension in σ_8* , *JCAP* **09** (2015) 067 [[1505.05511](#)].
- [51] G. Franco Abellán, R. Murgia, V. Poulin and J. Lavalley, *Implications of the S_8 tension for decaying dark matter with warm decay products*, *Phys. Rev. D* **105** (2022) 063525 [[2008.09615](#)].
- [52] R. Essig, E. Kuflik, S. D. McDermott, T. Volansky and K. M. Zurek, *Constraining Light Dark Matter with Diffuse X-Ray and Gamma-Ray Observations*, *JHEP* **11** (2013) 193 [[1309.4091](#)].
- [53] J. I. Read, *The Local Dark Matter Density*, *J. Phys.* **G41** (2014) 063101 [[1404.1938](#)].
- [54] D. A. Neufeld, G. R. Farrar and C. F. McKee, *Dark Matter that Interacts with Baryons: Density Distribution within the Earth and New Constraints on the Interaction Cross-section*, *Astrophys. J.* **866** (2018) 111 [[1805.08794](#)].
- [55] R. Cooke, M. Pettini, R. A. Jorgenson, M. T. Murphy and C. C. Steidel, *Precision measures of the primordial abundance of deuterium*, *Astrophys. J.* **781** (2014) 31 [[1308.3240](#)].
- [56] A. Coc, P. Petitjean, J.-P. Uzan, E. Vangioni, P. Descouvemont, C. Iliadis et al., *New reaction rates for improved primordial D/H calculation and the cosmic evolution of deuterium*, *Phys. Rev. D* **92** (2015) 123526 [[1511.03843](#)].
- [57] BELLE collaboration, *Search for an H -dibaryon with mass near $2m_\Lambda$ in $\Upsilon(1S)$ and $\Upsilon(2S)$ decays*, *Phys. Rev. Lett.* **110** (2013) 222002 [[1302.4028](#)].
- [58] KEK-PS E224 collaboration, *Enhanced Lambda Lambda production near threshold in the $C-12(K^-, K^+)$ reaction*, *Phys. Lett.* **B444** (1998) 267.
- [59] C. J. Yoon et al., *Search for the H -dibaryon resonance in $C-12$ (K^-, K^+ Lambda Lambda X)*, *Phys. Rev.* **C75** (2007) 022201.
- [60] BNL-E888 collaboration, *Search for diffractive dissociation of a longlived H dibaryon*, *Phys. Rev.* **D53** (1996) R3487.
- [61] BNL-E888 collaboration, *Search for the weak decay of an H dibaryon*, *Phys. Rev. Lett.* **76** (1996) 3277 [[hep-ex/9603002](#)].
- [62] BNL E836 collaboration, *Search for H dibaryon in $He-3$ (K^-, k^+) Hn* , *Phys. Rev. Lett.* **78** (1997) 3646.
- [63] A. T. M. Aerts and C. B. Dover, *THE (K^-, K^+) REACTION AND THE H DIBARYON*, *Phys. Rev. Lett.* **49** (1982) 1752.
- [64] A. t. m. Aerts and C. b. Dover, *ON THE PRODUCTION OF THE SIX QUARK H DIBARYON IN THE (K^-, K^+) REACTION*, *Phys. Rev. D* **28** (1983) 450.
- [65] N. Bar, K. Blum and G. D'Amico, *Is there a supernova bound on axions?*, *Phys. Rev. D* **101** (2020) 123025 [[1907.05020](#)].
- [66] N. Isgur and G. Karl, *Positive Parity Excited Baryons in a Quark Model with Hyperfine Interactions*, *Phys. Rev. D* **19** (1979) 2653.
- [67] G. R. Farrar and Z. Wang, *In preparation*, 2023.
- [68] R. Wiringa, *Private communication*, 2019.
- [69] M. Naghdi, *Nucleon-nucleon interaction: A typical/concise review*, *Phys. Part. Nucl.* **45** (2014) 924 [[nucl-th/0702078](#)].
- [70] T. Hamada and I. Johnston, *A potential model representation of two-nucleon data below 315 mev*, *Nuclear Physics* **34** (1962) 382.
- [71] J. Reid, Roderick V., *Local phenomenological nucleon-nucleon potentials*, *Annals of Physics* **50** (1968) 411.

- [72] D. Lonardoni, A. Lovato, S. C. Pieper and R. B. Wiringa, *Variational calculation of the ground state of closed-shell nuclei up to $A = 40$* , *Phys. Rev. C* **96** (2017) 024326 [[1705.04337](#)].
- [73] M. Shahrbafe, D. Blaschke, S. Typel, G. R. Farrar and D. E. Alvarez-Castillo, *Sexaquark dilemma in neutron stars and its solution by quark deconfinement*, *Phys. Rev. D* **105** (2022) 103005 [[2202.00652](#)].
- [74] T. Bringmann and M. Pospelov, *Novel direct detection constraints on light dark matter*, *Phys. Rev. Lett.* **122** (2019) 171801 [[1810.10543](#)].
- [75] J. Alvey, T. Bringmann and H. Kolesova, *No room to hide: implications of cosmic-ray upscattering for GeV-scale dark matter*, *JHEP* **01** (2023) 123 [[2209.03360](#)].
- [76] G. R. Farrar and X. Xu, *Limits on moderately-interacting Cosmic Ray Dark Matter in the GeV mass range in underground detectors*, [in preparation](#).
- [77] M. Cannoni, *Relativistic $\langle \sigma v_{\text{rel}} \rangle$ in the calculation of relics abundances: a closer look*, *Phys. Rev.* **D89** (2014) 103533 [[1311.4508](#)].
- [78] M. Thomson, *Modern Particle Physics*. Cambridge University Press, 2013.
- [79] P. McNamee, S. J. and F. CHILTON, *Tables of clebsch-gordan coefficients of su_3* , *Rev. Mod. Phys.* **36** (1964) 1005.
- [80] K. Scholberg, *Supernova Neutrino Detection*, *Ann. Rev. Nucl. Part. Sci.* **62** (2012) 81 [[1205.6003](#)].
- [81] A. Parreno, C. Bennhold and B. R. Holstein, *An EFT for the weak ΛN interaction*, *Nucl. Phys.* **A754** (2005) 127 [[nucl-th/0312047](#)].
- [82] PARTICLE DATA GROUP collaboration, *Review of Particle Physics*, *Phys. Rev.* **D98** (2018) 030001.